

# REFINED FINITE ELEMENT MODELLING OF CONCRETE-FILLED STEEL STUB COLUMNS

Zhong Tao<sup>1</sup>

**ABSTRACT:** A wide range of experimental data is collected in this paper and used to develop refined FE models to simulate concrete-filled steel tubular (CFST) stub columns under axial compression. The simulation is based on the concrete damaged plasticity material model, where a new strain hardening/softening function is developed for confined concrete and new models are introduced for a few material parameters used in the concrete model. The prediction accuracy from the current model is compared with that of an existing FE model, which has been well established and widely used by many researchers. The comparison indicates that the new model is more versatile and accurate to be used in modelling CFST stub columns, even when high-strength concrete and/or thin-walled tubes are used.

**KEYWORDS:** Concrete-filled steel tubes, axial compression, finite element analysis, passive confinement

## 1 INTRODUCTION

Due to the excellent composite action between the steel tube and concrete, concrete-filled steel tubular (CFST) columns are becoming increasingly popular and used in various structures throughout the world. Extensive experimental and analytical studies have been conducted to understand the behaviour of the composite columns mainly from the 1960s. From these investigations, different design codes have been formulated to reflect the design philosophies and practices in the respective countries, such as Australia, China, Japan, USA and European countries.

In recent decades, finite element (FE) technique is becoming increasingly popular for modelling CFST columns thanks to the existence of commercially available programs, such as ABAQUS and ANSYS. FE analysis allows the direct modelling of the composite action between the steel and concrete components, and different factors, such as local and global imperfections, residual stresses and boundary conditions, can be considered more precisely. The prediction accuracy of a FE model, however, is greatly affected by the input parameters, especially by the selection of a suitable concrete model.

Nowadays, high-performance construction materials, such as high-performance concrete and steel, are being increasingly used in engineering structures as a result of the continued advancement of materials technology. These high-performance materials often exhibit high strength. As far as CFST columns in real structures are concerned, the highest cylinder compressive strength and yield strength reported so far is 130 MPa and 690 MPa for the concrete and steel, respectively [1]. FE analysis is now used routinely for design and research problems. To embrace the development of materials, new FE models may need to be developed to improve the prediction

accuracy. To serve this purpose, sufficient test data needs to be collected and used to verify the prediction accuracy.

In the past, numerous tests have been conducted on CFST stub columns. A database was used by Tao et al. [2] to check the applicability of different codes in calculating the strength of CFST columns. In that database, 484 test results for circular stub columns and 445 test results for rectangular stub columns (square sections mainly) were included. Only ultimate strength, however, was reported in the literature for the majority of these test results. It is worth noting that different authors might give different definitions of the ultimate strength. This may affect the magnitudes of the ultimate strength, especially for those columns without softening post-yield response. Meanwhile, the capacity of predicting full-range load–deformation curves is also very important in evaluating FE models. In this paper, only test results of axial load ( $N$ )–axial strain ( $\varepsilon$ ) or axial shortening ( $\Delta$ ) curves reported are collected and used to make consistent comparisons.

Among many FE models, the FE model developed by Han et al. [3] has been widely used to simulate CFST columns, where the concrete damaged plasticity model in ABAQUS was adopted. Default values, however, were used in Han et al. [3] for many material parameters, such as the dilation angle ( $\psi$ ), the ratio of the compressive strength under biaxial loading to uniaxial compressive strength ( $f_{b0}/f_c'$ ), and the ratio of the second stress invariant on the tensile meridian to that on the compressive meridian ( $K_c$ ). This paper aims to develop a refined FE model in simulating CFST columns, in which new models, if required, will be introduced to determine these concrete material parameters. Meanwhile, a new strain hardening/softening rule will be developed for concrete. The wide range of test data collected will be used to calibrate the new FE model.

<sup>1</sup> Zhong Tao, Institute for Infrastructure Engineering, University of Western Sydney. Email: z.tao@uws.edu.au

## 2 FE MODELLING

### 2.1 GENERAL

The general-purpose finite element program ABAQUS version 6.12 was used in the present study to build a FE model for CFST stub columns. Four-node shell elements with reduced integration (S4R) and 8-node brick elements with three translation degrees of freedom at each node (C3D8R) were used to model the steel tube and concrete core, respectively.

Mesh convergence studies were conducted to determine optimal FE mesh to provide relatively accurate solution with low computational time. It was found that the aspect ratio of elements has negligible influence on the  $N-\epsilon$  curves if this ratio is smaller than 3. Therefore, element size in the axial direction was selected as 2.5 times that in the lateral direction. Based on the mesh convergence studies, element size across the cross-section was chosen as  $D/15$  for a circular column or  $B/15$  for a rectangular column, where  $D$  and  $B$  are the overall diameter of the circular tube and the overall width of the rectangular tube, respectively. For a typical specimen, the mesh contains a total of over 4000 elements.

Surface-to-surface contact is usually used for the interaction simulation of the steel tube and concrete. A contact surface pair comprised of the inner surface of the steel tube and the outer surface of concrete core can be defined. "Hard contact" in the normal direction can be specified for the interface, which allows the separation of the interface in tension and no penetration of that in compression. The tangent contact can be simulated by the Coulomb friction model. For CFST stub columns, there is little or no slip between the steel tube and concrete since they are loaded simultaneously. For this reason, the column's behaviour is not sensitive to the selection of friction coefficient between steel and concrete.

In the current FE model, the surface-based interaction continues to be used to model the concrete-steel tube interface. A coefficient of friction between the steel tube and concrete was taken as 0.6, which agrees with most test results [4].

The Poisson's ratios for steel and concrete were taken as 0.3 and 0.2, respectively. These values have been used widely in FE numerical simulation.

It has been well documented that initial local imperfections and residual stresses have apparent influence on the behaviour of hollow tubes. For CFST stub columns, however, the effects of local imperfections and residual stresses are minimised by concrete filling, and were therefore ignored in the current FE simulation. This was confirmed by the research conducted by Tao et al. [5], which explained that the out-of-plane deformation of the steel tube caused by the concrete expansion plays a similar role as the initial imperfections.

### 2.2 BOUNDARY CONDITIONS

A stub column was normally placed into a testing machine and the load was applied on the specimen directly. To minimise the influence of end conditions on CFST

stub columns, most researchers used end plates and/or stiffeners welded to both ends of a tube. Some tests, however, were conducted on specimens without end plates or stiffeners. If no stiffening method is used, local buckling of the steel tube is more likely to be initiated at the ends, which may affect the overall performance of the specimen.

For stub columns with welded end plates and/or stiffeners, there is no need to include the end plates or stiffeners in the model. Instead, the top and bottom surfaces of the steel tube and concrete can be fixed against all degrees of freedom except for the displacement at the loaded end (clamped end condition). The result obtained is the same as that of the model with end plates and/or stiffeners. For unstiffened stub columns, the steel and concrete are usually in direct contact with the stiff platens of the testing machine. Considering the end friction provided by the testing machine, all three translational degrees of freedom can be restrained for the ends of the column except the vertical displacement at the loaded end. The rotational degrees of freedom for both ends of the steel tube, however, are not restrained, which is referred to as pinned end condition. In most cases, the boundary conditions have very minor influence on  $N-\epsilon$  or  $N-\Delta$  curves. But some influence can be observed for square columns, especially when compact tubes are used. Figure 1 compares the obtained  $N-\Delta$  curves when pinned and clamped ends are used for the square specimen SSH-1-2 reported in [6]. The thickness of the end plates for this specimen is 20 mm, and other parameters are given in the figure, where  $B$  is the overall width of the square tube,  $t$  is the wall thickness,  $L$  is the specimen length,  $f_y$  and  $f'_c$  are the yield strength of steel and cylinder compressive strength of concrete, respectively. Computed local buckling occurs at the mid-height when a clamped support condition is used. But local buckling occurs only near the ends when a pinned support condition is used. In the latter case, the predicted ultimate strength decreases by 6.4% and the corresponding peak strain increases significantly, as shown in Figure 1. The comparison highlights that a stiffening method may be essential in some cases to eliminate/minimise the influence of end conditions.

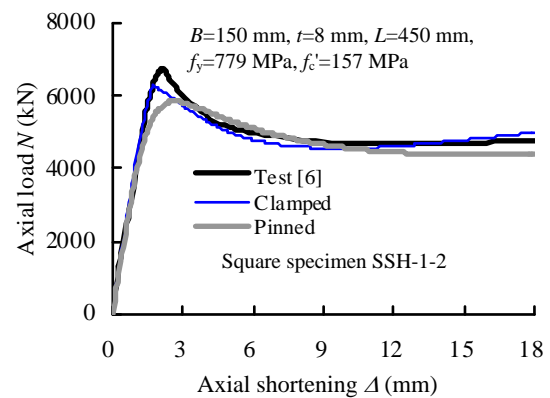


**Figure 1:** Influence of boundary conditions on predicted  $N-\Delta$  curves

In conducting tests, different  $L/D$  ratios of specimens were often used by different researchers. For columns with a larger  $L/D$  ratio, the global imperfections may somewhat affect the column's behaviour. A sensitivity analysis indicates that the ultimate strength decreases significantly when the  $L/D$  ratio increases from 1 to 1.5. This is owing to the fast diminishing end effects. When  $L/D$  ratios lie in the range of 2-5, very close  $N$ - $\varepsilon$  curves are obtained. Once the  $L/D$  ratio exceeds 5, obvious lateral deflection will develop and the ultimate strength begins to decrease again. Since  $L/D$  ratios reported in the past for almost all CFST stub columns are in the range from 2 to 5, the global imperfections can be ignored in a simulation.

### 2.3 MATERIAL MODELLING OF STEEL

Different stress ( $\sigma$ )-strain ( $\varepsilon$ ) models have been used for the steel material by different researchers, including elastic-perfectly plastic model, and elastic-plastic model with linear hardening or multi-linear hardening. At strains of general structural interest (normally less than 5%), steel exhibits no significant strain hardening. Very close axial load ( $N$ )-axial strain ( $\varepsilon$ ) curves are obtained using different stress-strain models for steel. In general, the selection of a  $\sigma$ - $\varepsilon$  relationship for steel has negligible influence on the ultimate strength and only affects the load-deformation curve slightly in a later stage.

In this paper, a model proposed by Tao et al. [7] was used to simulate the steel material in circular CFST columns, which is expressed as follows

$$\sigma = \begin{cases} E_s \varepsilon & 0 \leq \varepsilon < \varepsilon_y \\ f_y & \varepsilon_y \leq \varepsilon < \varepsilon_p \\ f_u - (f_u - f_y) \cdot \left( \frac{\varepsilon_u - \varepsilon}{\varepsilon_u - \varepsilon_p} \right)^p & \varepsilon_p \leq \varepsilon < \varepsilon_u \\ f_u & \varepsilon \geq \varepsilon_u \end{cases} \quad (1)$$

in which  $f_u$  is the ultimate strength;  $\varepsilon_y$  is the yield strain,  $\varepsilon_y = f_y/E_s$ ;  $\varepsilon_p$  is the strain at the onset of strain hardening;  $\varepsilon_u$  is the ultimate strain corresponding to the ultimate strength;  $p$  is the strain-hardening exponent. Equations are presented in Tao et al. [7] to determine  $p$ ,  $\varepsilon_p$ ,  $\varepsilon_u$  and  $f_u$ .

Unlike circular CFST columns, a rectangular CFST seldom demonstrates strain-hardening behaviour. This is owing to the easier local buckling of the rectangular steel tube and less effective confinement provided to the concrete. For this reason, an elastic-perfectly plastic model of steel gives a better prediction of the descending branch of the  $N$ - $\varepsilon$  curve than other models incorporating strain hardening. Therefore, the elastic-perfectly plastic model is used to simulate the steel material in rectangular CFST columns.

### 2.4 MATERIAL MODELLING OF CONCRETE

For a CFST column under axial compression, the concrete core expands laterally and is confined by the steel tube. This confinement is passive in nature, and can increase the strength and ductility of concrete. This mechanism is well understood and is often referred to as

“composite action” between the steel tube and concrete [3]. It is believed that the confined concrete is in a triaxial stress state and the steel is in a biaxial state after interaction between the two components occurs. FE analysis is a powerful method allowing the composite action to be considered provided a rational and accurate concrete model is available to describe the behaviour of concrete under passive confinement.

#### 2.4.1 Concrete damaged plasticity model

The concrete damaged plasticity model available in ABAQUS was used. Since this paper only deals with columns under monotonic loading, damage variables were not defined. Therefore, concrete nonlinearity was modelled as plasticity only. In this model, key material parameters to be determined include the ratio of the second stress invariant on the tensile meridian to that on the compressive meridian ( $K_c$ ), dilation angle ( $\psi$ ), and strain hardening/softening rule. Other parameters include the modulus of elasticity ( $E_c$ ), flow potential eccentricity ( $e$ ), ratio of the compressive strength under biaxial loading to uniaxial compressive strength ( $f_{bo}/f'_c$ ), viscosity parameter and tensile behaviour of concrete. For the FE model presented by Han et al. [3], constant values of  $30^\circ$ , 0.1, 1.16 and  $2/3$  were used for  $\psi$ ,  $e$ ,  $K_c$  and  $f_{bo}/f'_c$ , respectively. Considering the complex nature of passively confined concrete, constant values may not be suitable to be used in some cases. New models, if required, are introduced for these material parameters in the following sections.

The empirical equation (2) recommended in ACI 318 [8] was adopted to calculate  $E_c$ , where  $f'_c$  is in MPa. Default values of 0.1 and 0 were used for the flow potential eccentricity and viscosity parameter, respectively. These two parameters have no significant influence on the prediction accuracy.

$$E_c = 4700 \sqrt{f'_c} \quad (2)$$

Test results of equibiaxial concrete strength ( $f_{bo}$ ) are still very scarce. Based on test data collected from 14 references, Papanikolaou and Kappos [9] proposed the following equation to predict the ratio of  $f_{bo}/f'_c$ :

$$f_{bo}/f'_c = 1.5(f'_c)^{-0.075} \quad (3)$$

The above equation was used in this paper to determine the ratio of  $f_{bo}/f'_c$ . When the concrete strength  $f'_c$  is 30 MPa,  $f_{bo}/f'_c$  is 1.162 according to Equation (3). But when  $f'_c$  increases to 100 MPa,  $f_{bo}/f'_c$  drops to 1.062. In general, the calculated ultimate strength  $N_u$  will increase slightly if a higher ratio of  $f_{bo}/f'_c$  is used.

Although CFST stub columns are not sensitive to tensile behaviour of concrete when subjected to axial compression, tension stiffening needs to be defined in ABAQUS. In the current model, the uniaxial tensile response was assumed to be linear until the tensile strength of concrete was reached, which was taken as  $0.1f'_c$ . Beyond this failure stress, the tensile softening response was characterised by means of fracture energy ( $G_F$ ). The following equation was used to define  $G_F$  for tensile concrete [10]:

$$G_F = (0.0469d_{\max}^2 - 0.5d_{\max} + 26)\left(\frac{f_c'}{10}\right)^{0.7} \text{ N/m} \quad (4)$$

where  $f_c'$  is in MPa,  $d_{\max}$  is the maximum coarse aggregate size (in mm). If  $d_{\max}$  had not been reported in a reference, it was taken as 20 mm.

#### 2.4.2 Determining $K_c$

The ratio of the second stress invariant on the tensile meridian to that on the compressive meridian ( $K_c$ ) is one of parameters for determining the yield surface of concrete plasticity model. Test results indicate that the range of  $K_c$  varies from 0.5 to 1. The default value of  $K_c$  used in ABAQUS is 2/3, which has been adopted by many researchers. A sensitivity analysis was carried out to investigate the influence of  $K_c$  on  $N$ - $\varepsilon$  curves of a circular specimen tested by Tomii et al. [11]. The results of the sensitivity analysis are shown in Figure 2. It can be found that  $K_c$  has no influence on the initial stage of the  $N$ - $\varepsilon$  curve. After the yielding of the column, the influence of  $K_c$  becomes significant. The ultimate strength increases with decreasing  $K_c$ . This highlights that the value of  $K_c$  should be determined very carefully.

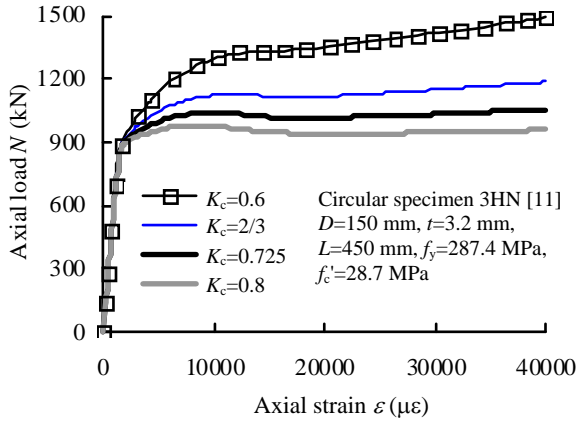


Figure 2: Influence of  $K_c$  on  $N$ - $\varepsilon$  curves

Assuming the ratio of  $f_{b0}/f_c'$  to be 1.16, it was derived by Yu et al. [12] that  $K_c$  could be taken as 0.725. Since  $f_{b0}/f_c'$  is expressed as a function of  $f_c'$  in this paper as shown in Equation (3),  $K_c$  will also be related to  $f_c'$ . According to Yu et al. [12], the following equation can be deduced to calculate  $K_c$ :

$$K_c = \frac{5.5f_{b0}}{3f_c' + 5f_{b0}} \quad (5)$$

By introducing Equation (3) into Equation (5),  $K_c$  can be determined by

$$K_c = \frac{5.5}{5 + 2(f_c')^{0.075}} \quad (6)$$

From this equation, it can be found that  $K_c$  decreases slightly from 0.725 to 0.703 when  $f_c'$  increases from 30 MPa to 100 MPa.

#### 2.4.3 Determining $\psi$

Dilation angle ( $\psi$ ) is one of parameters required for ABAQUS to define the plastic flow potential. The allowed value of  $\psi$  ranges from  $0^\circ$  to  $56^\circ$  in ABAQUS.

Different constant values of  $\psi$  have been used by different researchers in the past. Most researchers adopted a value of  $20^\circ$  or  $30^\circ$  for confined concrete.

The influence of  $\psi$  on  $N$ - $\varepsilon$  curves is shown in Figure 3 based on sensitivity analysis. Once again, the circular specimen tested by Tomii et al. [11] was used as an example. Four different  $\psi$  values were selected, i.e.,  $0.01^\circ$ ,  $20^\circ$ ,  $30^\circ$  and  $40^\circ$ . Since  $\psi$  cannot be taken as 0 in ABAQUS, a small value of  $0.01^\circ$  was used to represent this level. The dilation rate of concrete decreases with decreasing  $\psi$ , which affects the interaction between the steel tube and concrete. As  $\psi$  increases, stronger interaction will be developed and the concrete can be confined by a higher confining stress at a later stage. As a result of this, the computed ultimate strength increases with an increase in  $\psi$ . It is also found that the initial stage of the  $N$ - $\varepsilon$  curve is not affected by the selection of  $\psi$ .

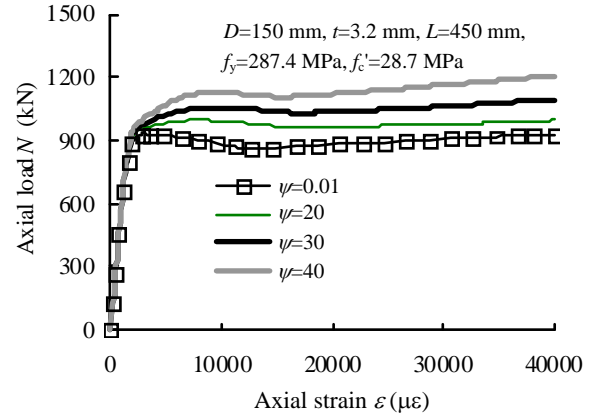


Figure 3: Influence of  $\psi$  on  $N$ - $\varepsilon$  curves

As pointed out by Yu et al. [13],  $\psi$  is affected by the confining stress and plastic deformation of concrete. For concrete confined by a steel tube, the variation in confining stress is less significant after the yielding of the steel tube. Since  $\psi$  does not affect the initial stage of the  $N$ - $\varepsilon$  curve, it is valid to assume a constant  $\psi$  for a column in calculating the full-range  $N$ - $\varepsilon$  curve. Since the dilation of concrete decreases with increasing confinement, it is assumed that  $\psi$  is a function of the so-called “confinement factor”  $\xi_c$ . Numerical tests were conducted to identify suitable values of  $\psi$  for specimens with different  $\xi_c$ . The following equation is then proposed based on regression analysis to determine  $\psi$  for circular columns.

$$\psi = \begin{cases} 56.3(1 - \frac{\xi_c}{7.4}) & \text{for } \xi_c \leq 0.5 \\ 6.672e^{\frac{4.64 + \xi_c}{7.4}} & \text{for } \xi_c > 0.5 \end{cases} \quad (7)$$

where the confinement factor  $\xi_c$  is expressed as

$$\xi_c = \frac{A_s f_y}{A_c f_c'} \quad (8)$$

in which  $A_s$  and  $A_c$  are the cross-sectional areas of the steel tube and concrete, respectively.

As far as rectangular columns are concerned, it is found that a constant value of  $40^\circ$  can be used for  $\psi$ . As mentioned earlier,  $N$ - $\varepsilon$  curves of rectangular columns are not very sensitive to  $\psi$  when  $\psi$  is greater than  $20^\circ$ . A value of

40° gives the best prediction of the ultimate strength for rectangular columns.

#### 2.4.4 Strain hardening/softening rule

For unconfined concrete under compression, the strain hardening/softening rule can be determined by the uniaxial  $\sigma$ - $\varepsilon$  curve of unconfined concrete. Almost identical slopes of strain softening branches, however, will be obtained if this  $\sigma$ - $\varepsilon$  curve continues to be used in ABAQUS for concrete confined by different constant active pressures [12]. This is not consistent with experimental observation that the descending branch becomes less steep when the confining pressure increases. To cope with this limitation of ABAQUS software, Yu et al. [12] pointed out that the hardening/softening function should be related not only to the plastic strain, but also to the confining pressure. A user-defined subroutine USDFLD was used by Yu et al. [12] to define the dependence of strain hardening/softening on the confining pressure for fibre reinforcement polymer (FRP)-confined concrete. To do this, a model is required to describe the axial strain-lateral strain relationship of concrete under various confining pressures.

For CFST columns under axial compression, it is believed that there is no or negligible interaction between the steel tube and concrete in the initial loading stage. A small gap may appear since the initial lateral expansion of the concrete is smaller than that of the steel tube due to the difference in Poisson's ratio between the steel and concrete. As axial strain increases, the lateral expansion of the concrete gradually becomes greater than the expansion of the steel until the two components are in contact again. After that, contact pressure and interaction develop between the steel tube and concrete. This mechanism highlights the complexity of the interaction in CFST columns. It is very difficult to measure the lateral expansion and confining pressure of concrete in a steel tube during the loading process. For this reason, no accurate model is available till now to describe the axial strain-lateral strain relationship of concrete in CFST columns.

Based on numerical tests, researchers proposed different compressive  $\sigma$ - $\varepsilon$  models to be used for FE modelling of concrete confined by steel tubes. These models can be used to determine the strain hardening/softening function directly. Therefore, no user-defined subroutine is required. This reduces the modelling complexity, increases the computation efficiency and avoids potential convergence problems.

Different from that proposed by Han et al. [3], a new three-stage model is proposed in this paper to represent the strain hardening/softening rule of concrete confined by steel tubes, as shown in Figure 4. In the initial stage (from Point O to Point A), there is no or very little interaction between the steel tube and concrete. Therefore, the ascending branch of the stress-strain relationship of unconfined concrete is appropriate to be used to represent the curve OA until the peak strength  $f'_c$  is reached. After that, a plateau (from Point A to Point B) is included to represent the increased peak strain of concrete

from confinement. During this stage, any strength increase of concrete from confinement will be captured in the simulation through the interaction between the steel tube and concrete. Beyond Point B, a softening portion with increased ductility resulting from confinement is defined.

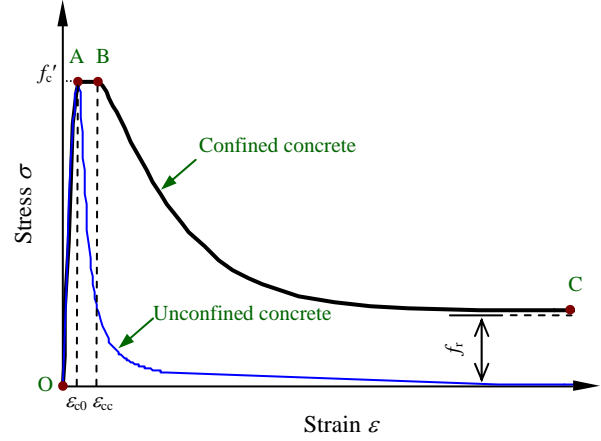


**Figure 4:** Stress-strain model proposed for confined concrete

A model proposed by Samani and Attard [14] is used to describe the ascending curve OA:

$$\frac{\sigma}{f'_c} = \frac{A \cdot X + B \cdot X^2}{1 + (A-2)X + (B+1)X^2} \quad 0 < \varepsilon \leq \varepsilon_{c0} \quad (9)$$

where  $X = \varepsilon/\varepsilon_{c0}$ ;  $A = \frac{E_c \varepsilon_{c0}}{f'_c}$ ;  $B = \frac{(A-1)^2}{0.55} - 1$ . The strain

at peak stress under uniaxial compression  $\varepsilon_{c0}$  is calculated according to the relationship in Equation (10). This equation was proposed by De Nicolo et al. [15] based on regression analysis of uniaxial compression tests results from 17 references, in which  $f'_c$  ranged from 10 MPa to 100 MPa.

$$\varepsilon_{c0} = 0.00076 + \sqrt{(0.626f'_c - 4.33) \times 10^{-7}} \quad (10)$$

where  $f'_c$  is expressed in MPa.

The strain at Point B ( $\varepsilon_{cc}$ ) for the concrete model is determined by the following equation proposed by Samani and Attard [14]:

$$\frac{\varepsilon_{cc}}{\varepsilon_{c0}} = e^k, \quad k = (2.9224 - 0.00367f'_c) \left( \frac{f_B}{f'_c} \right)^{0.3124 + 0.002f'_c} \quad (11)$$

where  $f_B$  is the confining stress provided to the concrete at Point B.

The circular specimen 3HN in Figure 2 is further used as an example to illustrate the development of confining stress on concrete ( $f_t$ ), which is shown in Figure 5. It should be pointed out that  $f_t$  is the average value at the interface between the steel tube and concrete. In the elastic stage, there is no confining stress as explained before. Just before and after the yielding of the steel, the confining stress increases very fast. Once the ultimate strength is reached,  $f_t$  keeps stable or increases very slowly depending on the value of  $\xi_c$ . This example highlights the fact that  $f_t$  changes with axial strain ( $\varepsilon$ ). To determine the

confining stress  $f_B$  corresponding to Point B in Figure 4, it is assumed that at this point the ultimate strength is reached, as shown in Figure 5.

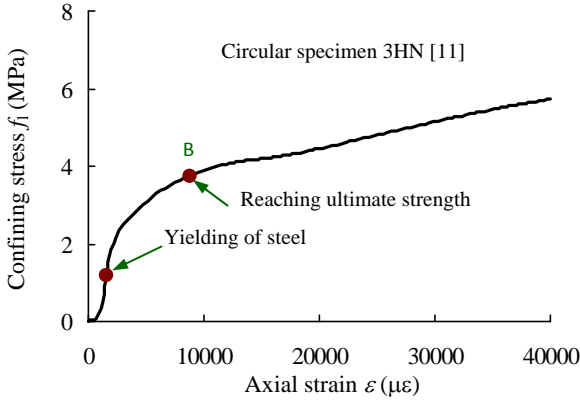


**Figure 5:** Development of confining stress ( $f_i$ ) as a function of axial strain ( $\varepsilon$ )

Numerical tests were conducted to calculate  $f_B$  for circular columns with different parameters. It is found that  $f_B$  increases with increasing  $f_y$  or decreasing  $D/t$  ratio. Although  $f_c'$  has no significant influence on the development of  $f_i$  in a later stage, there is a delay in the development of interaction and  $f_i$  for columns with higher strength concrete. Therefore,  $f_B$  also decreases with increasing  $f_c'$ . On the basis of regression analysis, Equation (12a) is proposed to determine  $f_B$  for circular columns. For rectangular CFST columns, the concrete core is subjected to uneven confinement, and  $f_i$  at the corners will be higher than those at other parts. It is found that a reduction factor of 0.25 can be applied to Equation (12a) for rectangular CFST columns and reasonable  $N-\varepsilon$  curves can be obtained. Therefore,  $f_B$  determining from Equation (12b) can be viewed as an equivalent confining stress.

$$f_B = \frac{(1 + 0.027f_y) \cdot e^{-0.02\frac{D}{t}}}{1 + 1.6e^{-10} \cdot (f_c')^{4.8}} \quad (\text{circular}) \quad (12a)$$

$$f_B = \frac{0.25 \cdot (1 + 0.027f_y) \cdot e^{-0.02\sqrt{(B^2 + D^2)/2} \cdot \frac{1}{t}}}{1 + 1.6e^{-10} \cdot (f_c')^{4.8}} \quad (\text{rectangular}) \quad (12b)$$

For the descending branch of the concrete model (BC) shown in Figure 4, an exponential function proposed by Binici [16] was used, which is defined by:

$$\sigma = f_r + (f_c' - f_r) \exp \left[ - \left( \frac{\varepsilon - \varepsilon_{cc}}{\alpha} \right)^\beta \right] \quad \varepsilon \geq \varepsilon_{cc} \quad (13)$$

in which  $f_r$  is the residual stress as shown in Figure 4;  $\alpha$  and  $\beta$  are parameters determining the shape of the softening branch. The expression for  $f_r$  is proposed as:

$$f_r = \begin{cases} 0.7(1 - e^{-1.38\xi_c})f_c' \leq 0.25f_c' & (\text{circular CFST}) \\ 0.1f_c' & (\text{rectangular CFST}) \end{cases} \quad (14)$$

The parameter  $\alpha$  is determined as:

$$\alpha = \begin{cases} 0.04 - \frac{0.036}{1 + e^{6.08\xi_c - 3.49}} & (\text{circular CFST}) \\ 0.005 + 0.0075\xi_c & (\text{rectangular CFST}) \end{cases} \quad (15)$$

Meanwhile,  $\beta$  can be taken as 1.2 and 0.92 for circular and rectangular columns, respectively. It should be noted that  $f_r$ ,  $\alpha$  and  $\beta$  cannot be derived from tests directly. Hence, different trial values were used until best-fit values were obtained to ensure predicted  $N-\varepsilon$  curves match with measured curves. It was found that  $f_r$  and  $\alpha$  can be expressed as functions of  $\xi_c$ . Equations (14) and (15) were then developed on the basis of regression analysis.

### 3 VERIFICATION OF THE CURRENT FE MODEL

Through an extensive literature search,  $N-\varepsilon$  or  $N-\Delta$  curves of 142 circular, 154 square and 44 rectangular specimens were collected and used to verify the proposed FE model. The 340 tests in total are from 30 references, in which the majority of them have received extensive citations.

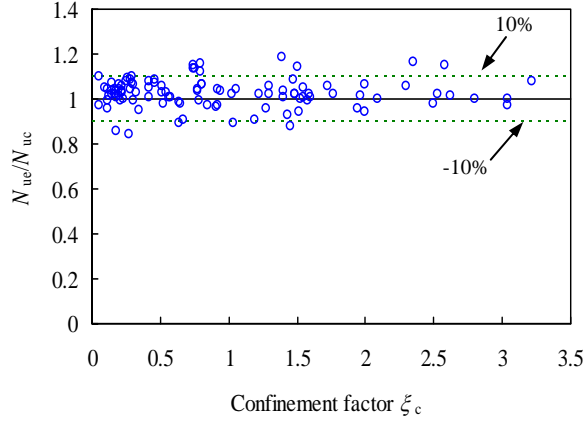
For circular columns, the ranges of different parameters are:  $f_y=186-853$  MPa;  $f_c'=18-185$  MPa;  $D=60-450$  mm,  $L/D=1.8-4.3$ , and  $D/t=17-221$ , where  $D$  is the overall diameter of a circular section. The parameter ranges for the rectangular columns are:  $f_y=194-835$  MPa;  $f_c'=13-164$  MPa;  $D=60-500$  mm,  $L/D=2.8-4.8$ ,  $D/t=11-150$ ; and  $D/B=1-2$ , where  $B$  and  $D$  are the overall width and depth of a rectangular section, respectively. As can be seen, the parameter ranges of the collected data are very broad and cover the current practical ranges. It should be noted that values of  $f_c'$  for some specimens were not available. Instead, a compressive strength ( $f_{cu}$ ) of 150 mm cubes was reported. To make consistent comparisons, Equation (16) proposed by L'Hermite [17] was used to convert  $f_{cu}$  to equivalent cylinder strength.

$$f_c' = \left[ 0.76 + 0.2 \log_{10} \left( \frac{f_{cu}}{19.6} \right) \right] f_{cu} \quad (16)$$

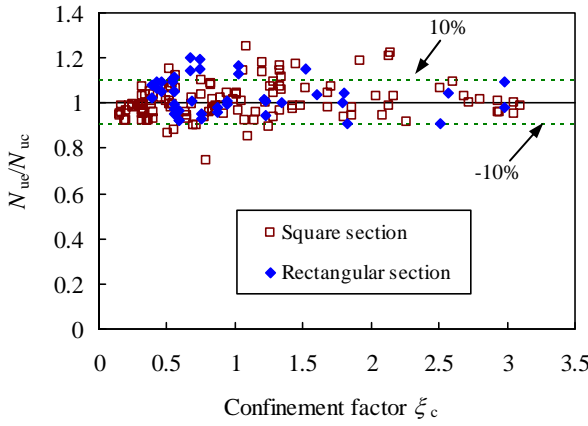
where  $f_c'$  and  $f_{cu}$  are both in MPa.

As observed from tests, peak loads for some stocky CFST specimens are often associated with very high plastic strains. In some cases, no descending branches of  $N-\varepsilon$  or  $N-\Delta$  curves can be observed. This is particularly true for circular columns. For comparison purposes, the ultimate strength ( $N_u$ ) is defined as the first peak load in this paper. But if the strain corresponding to the first peak load is great than 0.01 or there is no descending branch,  $N_u$  is then taken as the load at a strain of 0.01. It should be noted that  $\varepsilon$  was taken as  $\Delta/L$  if  $N-\Delta$  curves were reported instead of  $N-\varepsilon$  curves in some references.

The collected test data are used to verify the prediction accuracy of the current FE model. The predicted ultimate strengths ( $N_{uc}$ ) from the current FE model and Han et al.'s FE model are compared with the measured ultimate strengths ( $N_{ue}$ ) of all collected data in Figures 6 and 7, respectively. Table 1 shows both the mean value (Mean) and standard deviation (STD) of the ratio of  $N_{ue}/N_{uc}$  for specimens with different cross-sections.



(a) Circular section



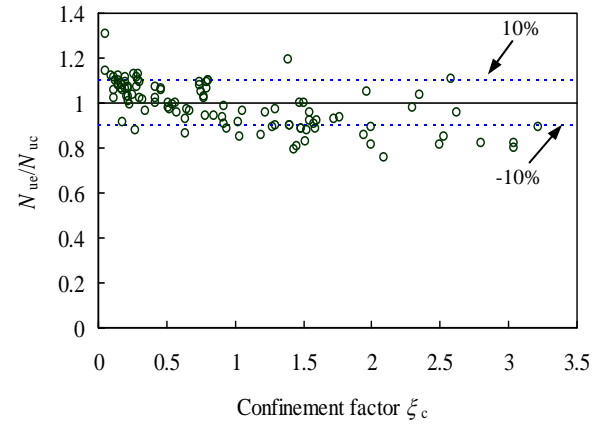
(b) Square and rectangular sections

**Figure 6:** Comparison between measured strength and predicted strength using current FE model

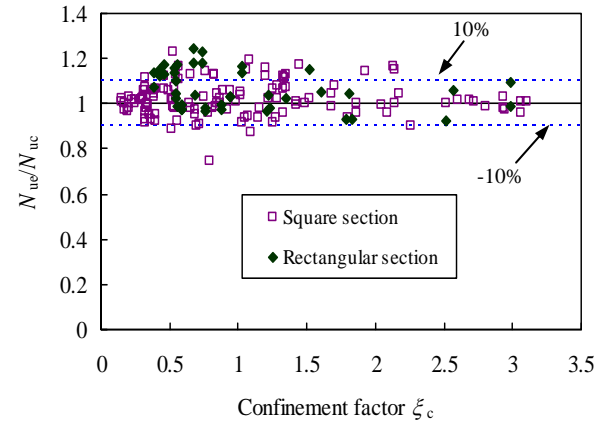
For the current FE model, the mean values of  $N_{ue}/N_{uc}$  are 1.024, 1.009 and 1.037 for circular, square and rectangular columns, respectively; whilst the standard deviations of  $N_{ue}/N_{uc}$  are 0.065, 0.078 and 0.079, respectively. As can be seen, slightly conservative predictions are obtained from the current FE model but with reasonable accuracy. For square columns, predictions of ultimate strengths from the new model are very close to those given by Han et al.'s model. But for circular and rectangular columns, the current model is superior to Han et al.'s model in predicting ultimate strength. In particular, Han et al.'s model underestimates the ultimate strengths of circular specimens with small  $\xi_c$  values, whilst overestimate those of circular specimens with large  $\xi_c$  values. This is owing to the fact that concrete in a circular tube is more effectively confined. It is expected that the confinement effect should be reflected in these material parameters, but instead constant material parameters were used by Han et al. [3] except the strain hardening/softening function. The current model gives good predictions for circular columns with either large or small  $\xi_c$  values, which can be seen from Figure 6a.

The influence of  $f_y$ ,  $f'_c$  and  $D/t$  ratio on prediction accuracy of the current FE model is further checked. In general, no change in prediction accuracy is found as  $f_y$ ,  $f'_c$  or the  $D/t$  ratio varies. The only exception is found regarding the influence of  $f'_c$  for square columns. A varia-

tion in prediction accuracy is found when the concrete strength is greater than 75 MPa. For example, the current FE model overestimates the ultimate strength by 7% on average for the 4 square specimens with an  $f'_c$  of 110 MPa reported by Varma [18]. On the other hand, Liew et al. [6] reported test results of 9 square columns, where the concrete strength  $f'_c$  varied from 148 MPa to 164 MPa. On average, the current model underestimates the ultimate strength by 15.5% for these specimens. Despite this, the shape of the descending branch of  $N-\varepsilon$  curves for these specimens is still predicted very well. A possible explanation of the variation in prediction accuracy is that high-strength concrete is very sensitive to curing conditions. It is very difficult to ensure the curing condition of concrete cylinders is the same as that of concrete inside a tube. To reduce the variation in strength, however, high-strength concrete cylinders may also be cured in a sealed condition and kept in a same environment as the specimens.



(a) Circular section



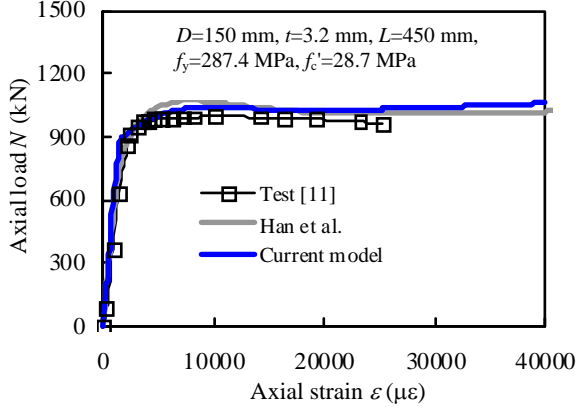
(b) Square and rectangular sections

**Figure 7:** Comparison between measured strength and predicted strength using Han et al.'s model

In terms of the prediction accuracy of  $N-\varepsilon$  curves, both the current FE model and Han et al.'s model give reasonable predictions for normal columns. This is illustrated in Figure 8, where the circular specimen 3HN tested by Tomii et al. [11] are used as examples. This explains why Han et al.'s model has been used widely.

**Table 1:** Comparison results of FE predictions with measured ultimate strength

Section type	Number of specimens	Han et al.'s model		Current FE model	
		Mean	STD	Mean	STD
Circular	142	0.989	0.098	1.024	0.065
Square	154	1.020	0.075	1.009	0.078
Rectangular	44	1.065	0.086	1.037	0.079



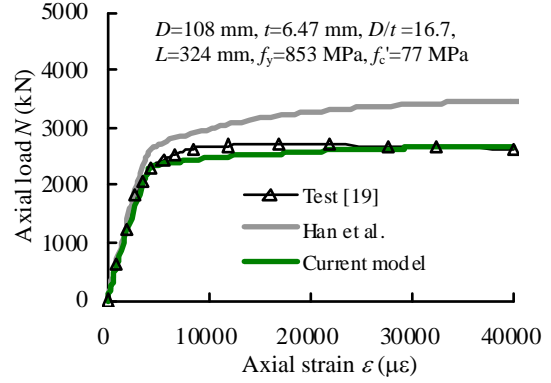
**Figure 8:** Comparison between predicted and measured  $N-\varepsilon$  curves for a circular specimen 3HN

Figure 9 shows the predicted  $N-\varepsilon$  curves of three specimens with stocky sections, including a circular specimen CC8-A-8 ( $D/t=16.7$ ), a square specimen sczs2-1-4 ( $B/t=20.5$ ) and a rectangular specimen No. 4 ( $D/t=28$ ) reported by Sakino et al. [19], Han et al. [20] and Lu and Kennedy [21], respectively. Han et al.'s FE model gives unsafe predictions of post-yielding strength for stocky circular columns as shown in Figure 9a. The predictions from the current FE model agree well with the test results of all the three specimens.

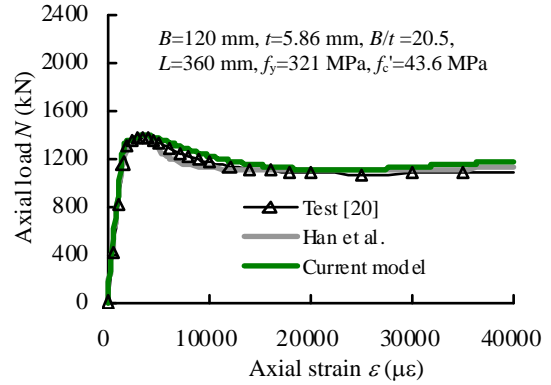
The predictions of Han et al.'s and the current FE models for specimens with thin-walled tubes and high-strength concrete are shown in Figures 10 and 11, respectively. The test curves of thin-walled specimens S16CS80A and UNC-H shown in Figure 10 were presented by O'Shea and Bridge [22] and Tao et al. [23], respectively; whilst those of specimens with high-strength concrete in Figure 11 were reported by Liew and Xiong [24], Liew et al. [6] and Liu and Gho [25], respectively. For circular thin-walled columns and circular CFST columns with high strength concrete, both models give reasonable predictions for the ultimate strength, but the current FE model is more satisfactory in predicting the strain softening branch than Han et al.'s FE model. For the  $N-\varepsilon$  curves of square or rectangular specimens shown in Figures 10 and 11, both models give reasonable predictions.

In general, the strain-hardening or softening branch is more accurately predicted using the current FE model. Meanwhile, the current model gives reasonably accurate predictions for columns in a wider parameter range. Apart from simulating normal CFST columns, the new FE model is also suitable to be used for CFST columns with high-strength concrete and/or thin-walled steel

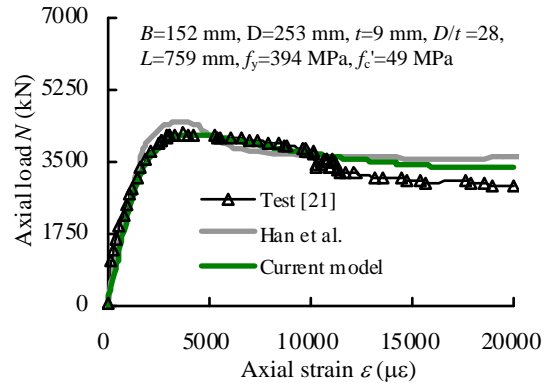
tubes. Compared with Han et al.'s model, the improvement of the current FE model in predicting the full-range  $N-\varepsilon$  or  $N-\Delta$  curves is more significant than the improvement in predicting the ultimate strength. This is especially true for circular specimens.



(a) Circular specimen CC8-A-8



(b) Square specimen sczs2-1-4

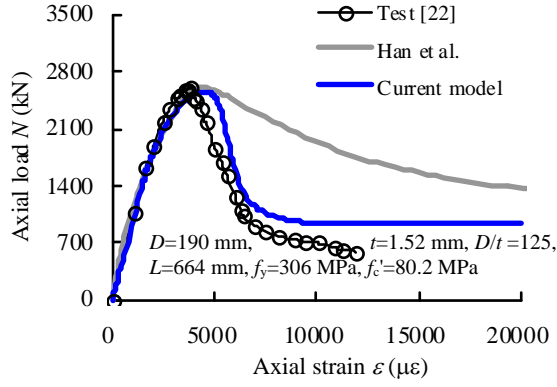


(c) Rectangular specimen No. 4

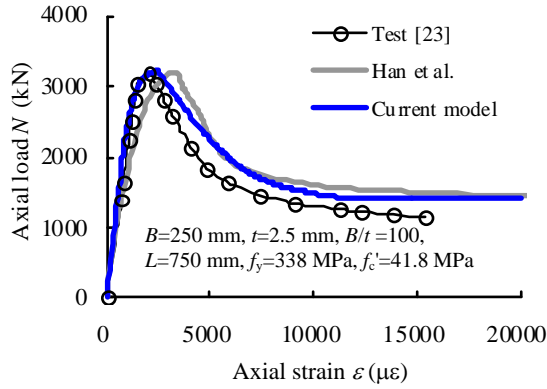
**Figure 9:** Comparison between predicted and measured  $N-\varepsilon$  curves for specimens with compact sections

## 4 CONCLUSIONS

In this paper, a wide range of experimental data was collected and used to develop a new FE model in simulating CFST stub columns under axial compression. This model was compared with an existing FE model developed by Han et al. [3] in terms of prediction



(a) Circular specimen S16CS80A



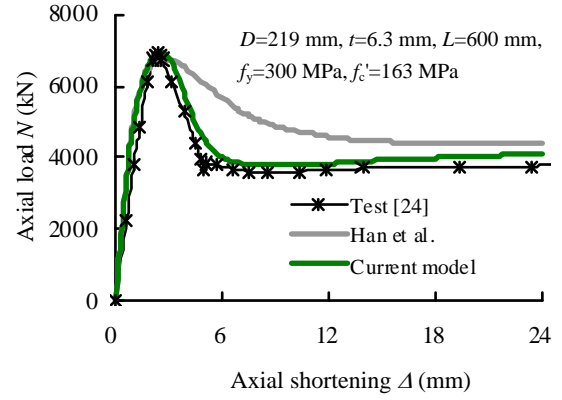
(b) Square specimen UNC-H

**Figure 10:** Comparison between predicted and measured  $N$ - $\varepsilon$  curves for concrete-filled thin-walled columns

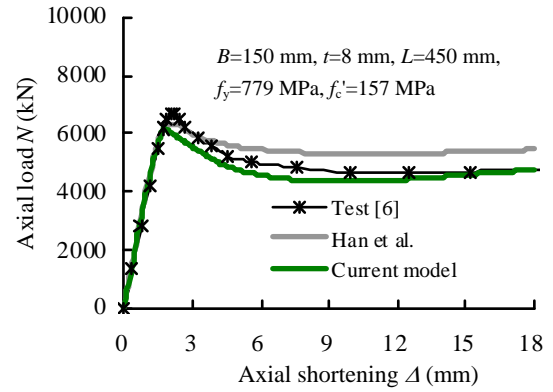
accuracy. The following conclusions can be drawn based on the results of this study:

- (1) Han et al.'s FE model gives reasonable predictions for normal CFST columns, although it underestimates the ultimate strengths of circular columns with small confinement factors  $\xi_c$ , and overestimates those of circular specimens with large  $\xi_c$  values. It was also found that the prediction of post-peak curves of circular columns with high-strength concrete or thin-walled tubes is less satisfactory using this model.
- (2) A new FE model was developed in this paper for CFST stub columns, where the dilation angle used in the concrete damaged plasticity model was calibrated against test data. Meanwhile, a new concrete strain hardening/softening function was developed to be used in modelling CFST columns.
- (3) The predictions from the new FE model were compared with the test data collected, which indicates that the new model is more versatile and accurate in modelling CFST stub columns. Apart from modelling normal CFST columns, the new FE model is also suitable to be used for CFST columns with high-strength concrete and/or thin-walled tubes.

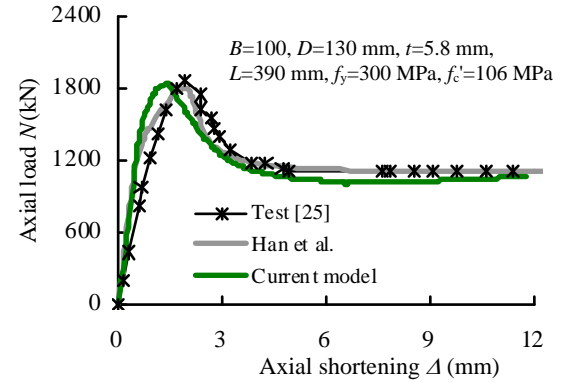
It should be noted that passively confined concrete is always very challenging to accurately model. The strain hardening/softening function for confined concrete



(a) Circular specimen CS-1



(b) Square specimen SSH-1-2



(c) Rectangular specimen A5-1

**Figure 11:** Comparison between predicted and measured  $N$ - $\Delta$  curves for CFST columns with high-strength concrete

should be related not only to the plastic strain, but also to the confining pressure. ABAQUS and most other software have a limitation in reflecting this. Further research is required to measure the lateral expansion of concrete inside a steel tube during the loading process. A model may be put forward accordingly to describe the axial strain-lateral strain relationship of the core concrete in CFST columns. A user-defined material subroutine can then be developed for ABAQUS to define a more rational strain hardening/softening function. In this way, the confining pressure between the steel tube and concrete can be determined from the interaction between the

two components, and the strain hardening/softening rule will not directly related to the geometric parameters of the cross-section.

## ACKNOWLEDGEMENTS

This work is supported by the Australian Research Council (ARC) under its Future Fellowships scheme (Project No: FT0991433). The financial support is highly appreciated.

## REFERENCES

- [1] Godfrey Jr. K. A. Concrete strength record jumps 36%. *Civil Eng*, ASCE, 57(10):84-86, 1987.
- [2] Tao Z., Uy B., Han L. H., He S. H. Design of concrete-filled steel tubular members according to the Australian Standard AS 5100 model and calibration. *Aust J Struct Eng*, 8(3):197-214, 2008.
- [3] Han L. H., Yao G. H., Tao Z. Performance of concrete-filled thin-walled steel tubes under pure torsion. *Thin-Walled Struct*, 45(1):24-36, 2007.
- [4] Rabbat B., Russell H. friction coefficient of steel on concrete or grout. *J Struct Eng*, ASCE, 111(3):505-515, 1985.
- [5] Tao Z., Uy B., Liao F. Y., Han L. H. Nonlinear analysis of concrete-filled square stainless steel stub columns under axial compression. *J Constr Steel Res*, 67(11):1719-1732, 2011.
- [6] Liew J. Y. R., Xiong D. X., Zhang M. H.: Experimental studies on concrete filled tubes with ultra-high strength materials. In *Proceedings of the 6th International Symposium on Steel Structures*, pages 377-384, 2011.
- [7] Tao Z., Wang X. Q., Uy B. Stress-strain curves of structural steel and reinforcing steel after exposure to elevated temperatures. *J Mater Civil Eng*, ASCE, 25(9):1306-1316, 2013.
- [8] American Concrete Institute. Building code requirements for structural concrete (ACI 318-11) and commentary. Farmington Hills, MI, USA, 2011.
- [9] Papanikolaou V. K., Kappos A. J. Confinement-sensitive plasticity constitutive model for concrete in triaxial compression. *Int J Solids Struct*, 44(21):7021-7048, 2007.
- [10] FIP. CEB-FIP Model Code 1990. Thomas Telford Ltd., London, 1993.
- [11] Tomii M., Yoshimura K., Morishita Y. Experimental studies on concrete filled tubular stub columns under concentric loading. In *Proceedings of the International Colloquium on Stability of Structures under Static and Dynamic Loads*, pages 718-741, 1977.
- [12] Yu T., Teng J. G., Wong Y. L., Dong S. L. Finite element modeling of confined concrete-I: Drucker-Prager type plasticity model. *Eng Struct*, 32(3):665-679, 2010.
- [13] Yu T., Teng J. G., Wong Y. L., Dong S. L. Finite element modeling of confined concrete-II: Plastic-damage model. *Eng Struct*, 32(3):680-691, 2010.
- [14] Samani A. K., Attard M. M. A stress-strain model for uniaxial and confined concrete under compression. *Eng Struct*, 41:335-349, 2012.
- [15] De Nicolo B., Pani L., Pozzo E. Strain of concrete at peak compressive stress for a wide range of compressive strengths. *Mater Struct*, 27(4):206-210, 1994.
- [16] Binici B. An analytical model for stress-strain behavior of confined concrete. *Eng Struct*, 27(7):1040-1051, 2005.
- [17] Mirza S. A., Lacroix E. A. Comparative strength analyses of concrete-encased steel composite columns. *J Struct Eng*, ASCE, 130(12):1941-1953, 2004.
- [18] Varma A. H. Seismic behavior, analysis, and design of high strength square concrete filled steel tube (CFT) columns. PhD Thesis, Department of Civil Engineering, Lehigh University, Bethlehem, Pennsylvania, USA, 2000.
- [19] Sakino K., Nakahara H., Morino S., Nishiyama I. Behavior of centrally loaded concrete-filled steel-tube short columns. *J Struct Eng*, 130(2):180-188, 2004.
- [20] Han L. H., Zhao X. L., Tao Z. Test and mechanics model for concrete-filled SHS stub columns, columns, and beam-columns. *Steel Compos Struct*, 1(1):51-74, 2001.
- [21] Lu Y. Q., Kennedy D. J. L. The flexural behaviour of concrete-filled hollow structural sections. *Can J Civil Eng*, 21(1):111-130, 1994.
- [22] O'Shea M. D., Bridge R. Q. Tests on circular thin-walled steel tubes filled with medium and high strength concrete. *Aust Civil Eng Trans*, 40:15-27, 1998.
- [23] Tao Z., Uy B., Han L. H., Wang Z. B. Analysis and design of concrete-filled stiffened thin-walled steel tubular columns under axial compression. *Thin-Walled Struct*, 47(12):1544-1556, 2009.
- [24] Liew J. Y. R., Xiong D. X. Ultra-high strength concrete filled columns for highrise buildings. In *Proceedings of the 4th International Conference on Steel & Composite Structures*, pages 82-93, 2010.
- [25] Liu D., Gho W. M. Axial load behaviour of high-strength rectangular concrete-filled steel tubular stub columns. *Thin-Walled Struct*, 43(8):1131-1142, 2005.